Topology-Guided Knowledge Distillation for Efficient Point Cloud Processing

Luu Tung Hai
The University of Alabama at Birmingham, USA
luutunghai@gmail.com

Thinh D. Le
Soongsil University, South Korea
thomlestudy295@gmail.com

Zhicheng Ding
Bowling Green State University, USA
dingz@bgsu.edu

Qing Tian
The University of Alabama at Birmingham, USA
qtian@uab.edu

Truong-Son Hy *
The University of Alabama at Birmingham, USA
thy@uab.edu

Abstract

Point cloud processing has gained significant attention due to its critical role in applications such as autonomous driving and 3D object recognition. However, deploying high-performance models like Point Transformer V3 in resource-constrained environments remains challenging due to their high computational and memory demands. This work introduces a novel distillation framework that leverages topology-aware representations and gradient-guided knowledge distillation to effectively transfer knowledge from a high-capacity teacher to a lightweight student model. Our approach captures the underlying geometric structures of point clouds while selectively guiding the student model's learning process through gradient-based feature alignment. Experimental results in the Nuscenes, SemanticKITTI, and Waymo datasets demonstrate that the proposed method achieves competitive performance, with an approximately 16× reduction in model size and a nearly 1.9× decrease in inference time compared to its teacher model. Notably, on NuScenes, our method achieves state-of-the-art performance among knowledge distillation techniques trained solely on LiDAR data, surpassing prior knowledge distillation baselines in segmentation performance. Our implementation is available publicly at: https://github.com/HySonLab/PointDistill.

1 Introduction

Point cloud data are a critical representation of 3D geometry and have become essential in a wide range of applications, from autonomous driving and robotic navigation to urban mapping [76, 11, 14, 46]. Recent advances in deep learning have enabled significant progress in point cloud processing, with models such as Point Transformer V3 [61] setting new benchmarks in accuracy and robustness. Despite the success of models like Point Transformer V3, their high computational demands and memory requirements [13, 3] pose challenges for deployment in resource-constrained environments, such as edge devices or real-time systems. To address this issue, various model compression strategies have been introduced, including methods such as network pruning [19, 40, 41], quantization [6, 10, 45], lightweight model architectures [26, 42], and knowledge distillation [69, 24, 70].

[*] Corresponding Author

Preprint. Under review.

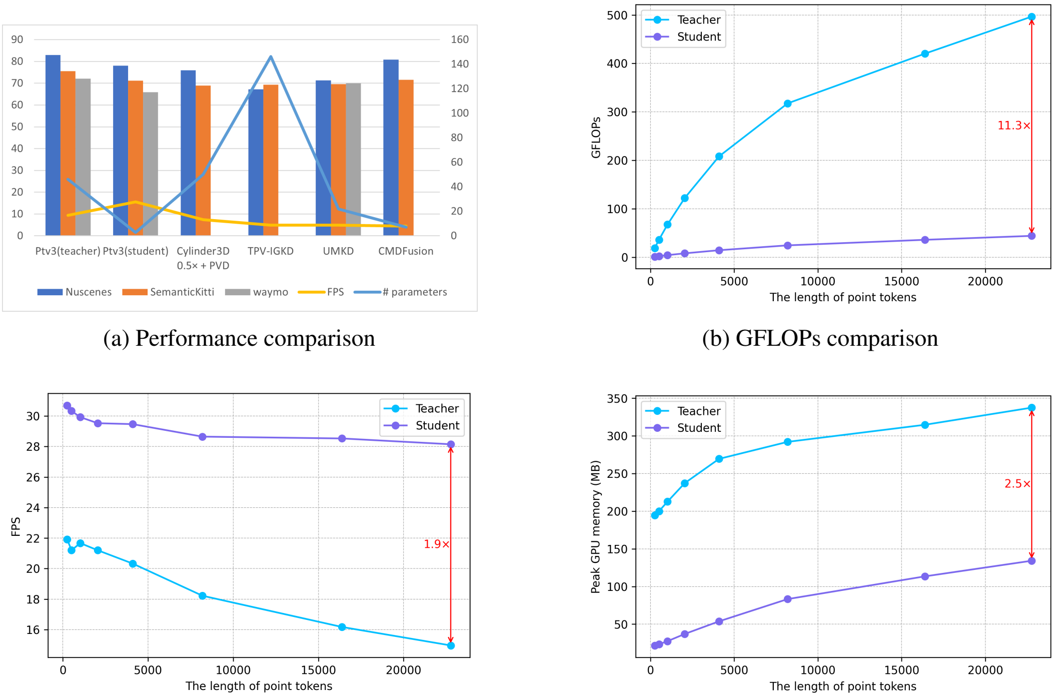

(a) Performance comparison

(b) GFLOPs comparison

(c) FPS comparison

(d) Peak Memory Comparison

Figure 1: Comprehensive comparisons between our proposed method and state-of-the-art knowledge distillation baselines across multiple evaluation metrics [23, 35, 55, 4]. (a) The radar chart demonstrates that our method achieves consistently better mIoU on three key datasets (NuScenes, SemanticKITTI, and Waymo), along with favorable FPS and memory efficiency. (b)-(d) As the input point token length increases, our approach maintains lower GPU memory usage and FLOPs, while sustaining significantly faster inference speed. (c) Peak GPU memory usage during inference, measured using max memory allocated function in Torch. This metric reflects the highest amount of memory used by the PyTorch tensors by the caching allocator during the inference phase. Notably, this value may differ significantly from the memory reported by the PyTorch Profiler due to its inclusion of temporary allocations used by CUDA kernels.

Knowledge distillation is a machine learning technique that aims to transfer knowledge from a large and high capacity model to a smaller and more efficient model [21, 51, 52]. This approach allows the student model to approximate the performance of the teacher while being computationally less demanding, making it suitable for deployment in resource-constrained environments such as edge devices or mobile platforms. Over the years, knowledge distillation has been effectively applied in various domains, including image recognition [51, 39] and natural language processing [17, 20, 49], demonstrating its versatility and impact. Recently, several approaches have been introduced to incorporate knowledge distillation into 3D detection tasks using point cloud data [16, 70]. Nevertheless, these methods primarily emphasize the selection of student-teacher models in a multimodal context, such as utilizing an image-based teacher to guide a point-cloud-based student detector or vice versa, while largely overlooking the distinctive characteristics of point clouds.

To address the challenges of current problems on point cloud distillation and the deployment of high-performance point cloud models in resource-constrained environments, we propose a novel distillation framework that combines topology-aware knowledge representation with gradient-guided distillation techniques. The framework leverages the inherent geometric and structural properties of point clouds to preserve critical topological information during the distillation process. By integrating gradient-based guidance, the proposed approach selectively emphasizes salient geometric features that contribute most significantly to the model's performance, enabling efficient knowledge transfer from a high-capacity teacher model to a lightweight student model. This strategy ensures that the student model retains competitive accuracy while significantly reducing computational and memory requirements, making it suitable for real-time and edge-based applications.

Extensive experiments on the proposed method have been conducted to demonstrate the effectiveness of our approach over previous knowledge distillation methods. Our main contributions can be summarized as follows.

- We propose a novel distillation framework that integrates topology-aware knowledge representation and gradient-guided distillation techniques, addressing the challenges of deploying high-performance point cloud models in resource-constrained environments.
- The framework leverages the unique geometric and structural properties of point clouds, embedding topological information into the distillation process to ensure the preservation of critical features necessary for accurate predictions.
- By incorporating gradient-guided distillation, our method selectively emphasizes salient features, enabling efficient and effective knowledge transfer from the teacher model to the student model.
- Extensive experimental results on popular benchmark datasets, such as Nuscenes reveal that our approach achieves up to a $16\times$ reduction in the number of parameters and a 77.75% reduction in CUDA memory consumption in linear operations and a $2.5\times$ lower in peak CUDA memory usage during inference while maintaining accuracy within 5% of state-of-the-art of non-distilled methods.

2 Related Works

2.1 3D Point Cloud Processing

The representation of 3D data using point clouds has become increasingly prominent in domains such as autonomous driving, robotics, and 3D reconstruction. Traditional deep learning approaches for understanding 3D point clouds can be categorized into three main types: projection-based, voxel-based, and point-based methods [18]. Projection-based techniques map 3D points onto 2D image planes and employ 2D CNN backbones for feature extraction[5, 33, 34], often losing geometric details in the process. Voxel-based methods convert point clouds into structured voxel grids, allowing 3D convolutions with sparse convolution enhancing efficiency[7, 53, 60], though they encounter scalability issues due to limited grid resolution, sparse and irregular data distribution, and kernel size constraints. In contrast, point-based methods directly process raw point clouds[43, 47, 57, 73], with early approaches struggling to capture local structures until recent transformer-based architectures improved performance by modeling long-range dependencies and adapting to irregular distributions[15, 50, 62, 66]. Furthermore, hybrid methods that integrate point-voxel or graph-based representations have emerged to balance accuracy and efficiency. Across these approaches, challenges such as noise, occlusion, and varying point density in real-world data continue to impact performance.

2.2 Point Transformer Architecture

Transformer architectures improve point-based methods by leveraging self-attention to capture local and global dependencies effectively, outperforming CNN-based and voxel-based approaches. Early models like PCT [15] and Point Transformer [62] demonstrated strong performance in classification and segmentation tasks.

Point Transformer V1 (PTv1) [74] extended the transformers to unordered 3D point sets by vector self-attention and local attention based on kNN, improving spatial modeling, but suffering from high memory and computational costs. Point Transformer V2 (PTv2) [63] introduced group vector attention and grid-based grouping to enhance scalability and reduce parameters, although kNN remained a bottleneck limiting long-range dependency capture.

Point Transformer V3 (PTv3) [61] shifted toward simplicity by serializing point clouds using space-filling curves and employing serialized patch attention, greatly expanding receptive fields, and eliminating kNN dependence. PTv3 achieved a $3.3\times$ speedup and a $10.2\times$ memory reduction over PTv2, establishing state-of-the-art results in diverse 3D tasks. However, PTv3's preprocessing overhead, increased latency on dense clouds, and dependence on high-end hardware limit its applicability in real-time, resource-constrained scenarios.

2.3 Knowledge Distillation

Knowledge distillation (KD) is a model-independent technique that improves student model training by transferring knowledge from a pre-trained teacher model, offering a way to enhance the efficiency of models such as Point Transformer V3 (PTv3). Early KD methods [22] matched softmax outputs for classification, while later studies [39, 51, 58] extended KD to intermediate layers, capturing richer geometric and contextual information crucial for point-cloud data. KD is particularly promising for addressing the challenges of PTv3 in real-time deployment by enabling lighter, faster models.

Topological Distillation leverages topological data analysis (TDA) to transfer global structural features. Methods like TGD [27] and TopKD [28] distill topological knowledge through persistence images (PI) and diagrams (PD), improving the alignment of student-teacher. Despite benefits, topological distillation faces scalability challenges due to the computational cost of TDA and potential errors from PD-to-PI approximations. Its effectiveness across diverse point cloud tasks and noisy data remains limited, requiring further research for maturity.

3 Methodology

3.1 Overview of the Framework

Our framework proposes a distillation approach to develop lightweight student models for point-cloud processing, targeting both output replication and internal representation alignment. As illustrated in Figure 2, the teacher model is a pre-trained high capacity point cloud network that extracts rich semantic and geometric features.

The student model is trained to emulate the teacher's behavior through two proposed mechanisms:

- **Topological Distillation**: Both teacher and student feature representations undergo Topological Data Analysis (TDA) to capture global structural information. Chamfer loss is applied to align the topological signatures, encouraging the student to preserve critical geometric structures.
- **Gradient-Guided Feature Alignment**: Feature maps are compared from the teacher and student, where gradients with respect to the features guide the alignment process.

3.2 Topology-Aware Distillation Learning

Traditional knowledge distillation focuses on aligning Euclidean feature maps, which may fail to capture the structural and geometric relationships inherent in 3D point clouds. To address this, we introduce a topology-aware distillation framework that ensures the student model preserves essential topological structures.

Given a point cloud $X \in \mathbb{R}^{N\times 3}$, we construct a simplicial complex $\mathcal{K}(X)$ through Vietoris-Rips filtration and extract persistence diagrams D_T and D_S for the teacher and the student, respectively. We then define a topology loss based on the Chamfer Distance between persistence diagrams:

$$\mathcal{L}_{\text{topo}} = \mathcal{L}_{\text{CD}}(D_T, D_S). \tag{1}$$

This topology loss serves as a regularizer, promoting topological consistency between teacher and student models without overwhelming feature-based alignment objectives. We further bound the gradient of $\mathcal{L}_{\text{topo}}$ to ensure a stable optimization. A theoretical justification and detailed discussion comparing Chamfer Distance and Wasserstein Distance are provided in Appendix C.

3.3 Gradient-Guided Knowledge Distillation

To ensure that the student model learns the most task-relevant features from the teacher and inspired from [32], we propose a gradient-guided feature alignment mechanism for the semantic segmentation task that leverages the gradients of the task-specific loss to prioritize important features during distillation. Formally, we define the importance weight of the k-th feature channel at layer l as:

$$w_l^k = \frac{1}{N}\sum_{i=1}^{N}\left|\frac{\partial \mathcal{L}_{\text{task}}}{\partial F_{i,k}^{l}}\right|, \tag{2}$$

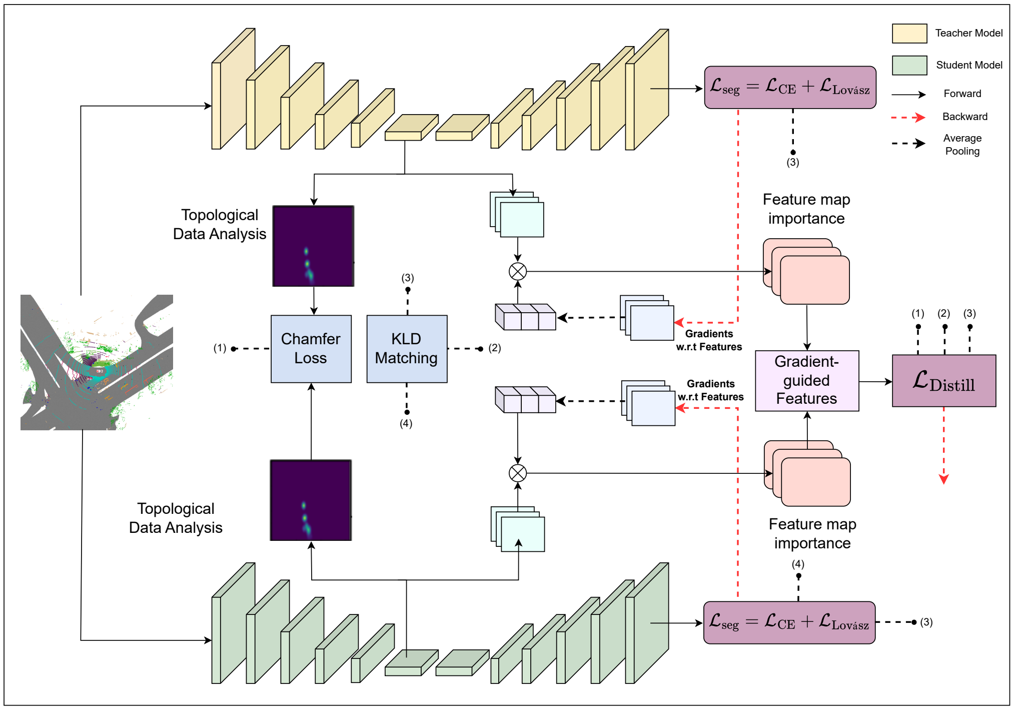
Teacher Model
Student Model
Forward
Backward
Average Pooling
$\mathcal{L}_{\text{seg}} = \mathcal{L}_{\text{CE}} + \mathcal{L}_{\text{Lovász}}$
(3)
Feature map importance
Topological Data Analysis
(3)
Chamfer Loss
KLD Matching
(1)
(2)
(4)
Gradients w.r.t Features
Gradients w.r.t Features
Gradient-guided Features
(1) (2) (3)
$\mathcal{L}_{\text{Distill}}$
Feature map importance
Topological Data Analysis
(4)
$\mathcal{L}_{\text{seg}} = \mathcal{L}_{\text{CE}} + \mathcal{L}_{\text{Lovász}}$
(3)

Figure 2: Overview of the proposed knowledge distillation framework for point cloud processing. The framework transfers knowledge from a teacher model (yellow) to a student model (green) using topological data analysis (TDA) (1), KLD matching (2), student semantic segmentation loss (3), and gradient-guided feature alignment (4). The total loss is the combination of (1), (2), (3) and gradient-guided feature loss.

where $\mathcal{L}_{\text{task}}$ is the task loss (e.g., cross-entropy for semantic segmentation), and $F^l_{i,k} \in \mathbb{R}$ is the feature activation for point i, channel k, and layer l. These gradients are averaged over all N points to obtain a channel-wise importance score. We then scale the feature representations for each point and channel:

$$\tilde{F}^l_{i,k} = w^k_l F^l_{i,k}. \tag{3}$$

Next, we compute a gradient-weighted feature map by aggregating the absolute values of the scaled features across all C channels for each point:

$$M^l_i = \sum_{k=1}^{C} |\tilde{F}^l_{i,k}|, \quad M^l = \text{Norm}([M^l_1, M^l_2, \ldots, M^l_N]), \tag{4}$$

where Norm is min-max normalization, defined as $\text{Norm}(x_i) = \frac{x_i - \min(x)}{\max(x) - \min(x)}$ for a vector $x = [x_1, \ldots, x_N]$. The resulting feature maps for the teacher and the student are denoted M^l_T and M^l_S, respectively. The gradient-guided feature alignment loss is then:

$$\mathcal{L}_{\text{grad}} = \frac{1}{N} \sum_{l=1}^{L} \sum_{i=1}^{N} \left| M^l_{i,T} - M^l_{i,S} \right|. \tag{5}$$

This loss encourages the student to align its task-relevant features with the teacher's, improving the effectiveness of knowledge transfer in 3D point cloud semantic segmentation.

3.4 Overall Distillation Objective

To complement the alignment based on topological and saliency, we incorporate Kullback-Leibler divergence (KLD) [30] to improve the consistency of the distribution level between teacher and student. By applying KLD to softened output logits or intermediate features, the student is guided to mimic not only the teacher's predictions but also the underlying confidence distribution, which helps capture class relationships and enhances generalization.

By incorporating multiple feature alignment strategies, the overall distillation objective integrates topology-aware feature transfer, gradient-guided feature alignment, distribution-level matching via KLD, Chamfer distance-based distribution matching, and segmentation loss. The final distillation loss is formulated as follows:

$$\mathcal{L}_{\text{Distill}} = \mathcal{L}_{\text{topo}} + \lambda_1 \mathcal{L}_{\text{grad}} + \lambda_2 \mathcal{L}_{\text{KLD}} + \lambda_3 \mathcal{L}_{\text{seg}}, \tag{6}$$

where:

- $\mathcal{L}_{\text{topo}}$ enforces the preservation of high-level topological structures between teacher and student models.
- $\mathcal{L}_{\text{grad}}$ ensures that the most important and informative features are transferred effectively.
- $\mathcal{L}_{\text{KLD}}$ minimizes the discrepancy between the feature distributions using the Kullback-Leibler divergence.
- $\mathcal{L}_{\text{seg}}$ represents the standard segmentation loss, ensuring that the student maintains an accurate point classification.

The hyperparameters λ_1, λ_2, and λ_3 control the relative importance of each loss component. By optimizing this composite objective, the student model is guided to capture both the **global topological** and **local geometric** properties, enhancing its generalization capability in point cloud tasks.

4 Experiments and Results

To assess our topology-aware distillation framework, we performed experiments on three prominent autonomous driving datasets: SemanticKITTI [1], Waymo Open Dataset [2], and NuScenes [54]. These datasets offer large-scale, real-world point-cloud sequences, ideal for benchmarking point-cloud processing techniques. We provide detailed descriptions of the datasets, training protocols, and evaluation procedures in the Appendix A.

4.1 Experimental Results

Comparison with previous state-of-the-art LiDAR semantic segmentation models. The results in Table 1 highlight the performance of various previous LiDAR semantic segmentation methods compared to our proposed distillation approach on the nuScenes test dataset, with mIoU scores ranging from 65.5% (RangeNet++) [44] to 78.17% (Student with KD). Among these methods, SDSeg3D [36] achieved the highest mIoU (77.7%), followed closely by RPVNet [64] (77.6%) and GFNet [48] (77.6%). In particular, the knowledge-distilled (KD) version of the student model surpassed all previous approaches with 78.17% mIoU, demonstrating the effectiveness of knowledge distillation in improving segmentation accuracy. However, despite these advances, all these models still have a lower performance than Point Transformer V3 [61], which achieves 83% mIoU on the nuScenes test dataset, setting a new benchmark in LiDAR semantic segmentation.

Comparison with state-of-the-art LiDAR knowledge distillation semantic segmentation models. The results in Table 1a compare various knowledge distillation methods on the nuScenes dataset, FPS and the number of parameters. Point Transformer V3 (teacher) achieves the highest performance with 83% mIoU, but has a relatively high parameter count (46.16M) and a lower FPS (16.61). Among student models, CMDFusion[4] achieves the highest mIoU (80.8%), coming closest to the teacher model while maintaining a significantly lower parameter count (7.04M) and FPS of 8. Our proposed distilled version reaches 78.01% mIoU, outperforming Cylinder3D 0.5× + PVD [23] (76%) and all other models based on KD. Additionally, it has the highest FPS (27.64), making it the most efficient model in terms of speed, while also being the most lightweight (2.78M parameters). Cylinder3D 0.5× + PVD [23] and TPV-IGKD [35] fall behind in terms of mIoU, with 76% and 67.2%, respectively, while also having significantly larger model sizes (50M and 146.18M). UMKD [55] achieves 71.3% mIoU, slightly outperforming TPV-IGKD, but with a smaller parameter count (21.8M). In general, our proposed KD method balances accuracy, speed, and efficiency better than other knowledge distillation methods.

Methods	**mIoU**	barrier	bicycle	bus	car	construction	motorcycle	pedestrian	traffic-cone	trailer	truck	driveable	other	sidewalk	terrain	manmade	vegetation
RangeNet++ [44]	65.5	66.0	21.3	77.2	80.9	30.2	66.8	69.6	52.1	54.2	72.3	94.1	66.6	63.5	70.1	83.1	79.8
PolarNet [72]	71.0	74.7	28.2	85.3	90.9	35.1	77.5	71.3	58.8	57.4	76.1	96.5	71.1	74.7	74.0	87.3	85.7
SalsaNext [9]	72.2	74.8	34.1	85.9	88.4	42.2	72.4	72.2	63.1	61.3	76.5	96.0	70.8	71.2	71.5	86.7	84.4
Cylinder3D [77]	76.1	76.4	40.3	91.2	93.8	51.3	78.0	78.9	64.9	62.1	84.4	96.8	71.6	76.4	75.4	90.5	87.4
C3D_0.5× + KA [25]	73.9	74.2	36.3	88.5	87.6	47.1	76.9	78.3	63.5	57.6	83.4	94.9	70.3	73.8	73.2	88.4	86.3
AMVNet [38]	76.1	79.8	32.4	87.4	90.4	62.5	81.9	75.3	72.3	83.5	65.1	97.4	67.0	78.8	74.6	90.8	87.9
2DPASS [65]	76.2	75.3	43.5	95.3	91.2	54.5	78.9	78.2	62.1	70.0	84.2	96.3	73.2	74.2	74.9	89.8	85.9
SDSeg3D [36]	77.7	77.5	49.4	93.9	92.5	54.9	86.7	80.1	67.8	65.7	86.0	96.4	74.0	74.9	74.5	86.0	82.8
RPVNet [64]	77.6	78.2	43.4	92.7	93.2	49.0	85.7	80.6	66.9	69.4	80.5	96.9	73.5	75.9	76.0	90.6	88.9
GFNet [48]	76.1	81.1	31.6	76.0	90.5	60.2	80.7	75.3	71.8	82.5	65.1	97.8	67.0	80.4	76.2	91.8	88.9
SVASeg [75]	74.7	74.1	44.5	88.4	86.6	48.2	72.4	72.3	61.3	57.5	75.7	96.3	70.7	74.7	74.6	87.3	86.9
Student w.o KD	76.08	76.14	46.66	89.99	92.18	40.36	83.90	78.35	63.18	68.18	81.74	96.32	72.78	73.65	75.39	89.72	88.77
Student with KD	**78.17**	**79.11**	**48.28**	**92.87**	**94.31**	**41.29**	**85.68**	**82.93**	**62.36**	**70.21**	**80.27**	**96.75**	**76.35**	**74.22**	**78.84**	**90.87**	**89.30**

Table 1: Comparison of our proposed method with previous state-of-the-art LiDAR semantic segmentation methods on the nuScenes test dataset. The table reports the mean Intersection over Union (mIoU) for different models across various object categories.

Methods	mIoU	car	bicycle	motorcycle	truck	other-vehicle	person	bicyclist	motorcyclist	road	parking	sidewalk	other-ground	building	fence	vegetation	trunk	terrain	pole	traffic
SalsaNext [9]	59.5	91.9	48.3	38.6	38.9	31.9	60.2	59.0	19.4	91.7	63.7	75.8	29.1	90.2	64.2	81.8	63.6	66.5	54.3	47.4
KPConv [57]	58.8	96.0	32.0	42.5	33.4	44.3	61.5	61.6	11.8	88.8	61.3	72.7	31.6	95.0	64.2	84.8	69.2	69.1	56.4	47.4
FusionNet [68]	61.3	95.3	47.5	37.7	41.8	34.5	59.5	56.8	11.9	91.8	68.7	77.1	30.5	90.5	69.4	84.5	69.8	68.5	60.4	46.2
KPRNet [29]	63.1	95.5	54.1	47.9	23.6	42.6	65.9	65.0	16.5	93.2	73.9	80.6	30.2	91.7	64.8	85.7	69.8	71.2	58.7	64.1
TORNADONet [12]	63.1	94.2	51.2	48.1	40.0	38.2	63.6	60.1	34.9	89.7	66.7	74.5	28.7	91.3	65.8	85.6	71.5	70.1	58.0	49.2
SPVNAS [56]	66.4	97.3	51.5	50.8	59.8	58.8	65.7	62.5	43.7	90.2	67.6	75.2	16.9	91.3	65.9	86.1	73.4	71.0	64.6	66.9
Cylinder3D [77]	68.9	97.1	67.6	50.8	50.8	58.5	73.7	69.2	48.0	92.2	65.0	77.0	32.3	90.7	66.5	85.6	72.5	69.8	62.4	66.2
Student w.o KD	69.5	98.0	68.9	52.4	52.4	59.9	74.9	70.5	49.6	93.2	66.4	78.2	34.1	91.7	67.8	86.7	73.7	71.1	63.8	67.6
Student with KD	**74.6**	**98.3**	**74.1**	**60.3**	**60.3**	**66.6**	**79.1**	**75.4**	**58.0**	**94.3**	**72.0**	**81.8**	**45.1**	**93.1**	**73.2**	**88.9**	**78.1**	**75.9**	**69.8**	**73.0**

Table 2: Comparison of semantic segmentation performance on the SemanticKITTI dataset. The table reports the mean Intersection over Union (mIoU) for different models across various object categories.

We further evaluate our method on the Waymo benchmark in Table 4. Among methods that use both LiDAR and camera inputs (LC), UMKD (SwiftNet34)(B) achieves the highest validation mIoU of 73.0, while MSeg3D slightly leads on the test set with 70.5. In contrast, methods that use only LiDAR (L) show competitive results, with LidarMultiNet [67] achieving the best validation performance of 73.8, surpassing all other methods, including those that use both modalities. However, this approach uses 3D bounding boxes as an additional supervision signal during training. Our proposed student model also performs well with a test mIoU of 71.3 and comparable validation performance with superiority in model parameter size (110.6M vs 2.78M), indicating strong generalization even when using only LiDAR data.

4.2 Comprehensive Teacher - Student Analysis

Tables 5 and 6 compare the Teacher (46.16M params) and Student (2.78M params) models in NuScenes, showcasing the efficiency benefits of knowledge distillation for semantic segmentation. The Teacher model, with 16.6× more parameters than the Student, has a deeper architecture suited for high-accuracy tasks on powerful hardware. In contrast, the Student's lightweight design, featuring fewer encoder and decoder blocks, attention heads, and channels, significantly reduces computational overhead. Specifically, the Student achieves a 36.70× reduction in encoder FLOPs and a 37.63× decrease in total attention compute, reflecting its streamlined transformer architecture. This efficiency

Method	**Parameters (Millions)**	**FPS**
RangeNet++ [44]	50.0	12.5
PolarNet [72]	45.0	16.7
SalsaNext [9]	6.7	23.8
Cylinder3D [77]	53.0	12.0
SalsaNext [9]	6.7	25.0
KPConv [57]	15.0	12.0
TornadoNet [12]	N/A	N/A
SPVNAS [56]	1.0	16.0
PTv3 (Teacher)	46.16	16.61
Our Student	**2.78**	**27.64**

Table 3: Comparison of the number of parameters (in millions) and inference speed (frames per second, FPS) for different LiDAR semantic segmentation methods on Nuscenes.

Method	**Input**	**mIoU** (test / val)
MSeg3D [37]	LC	70.5 / 69.6
UMKD (B) [55]	LC	70.0 / 71.1
UMKD (SwiftNet34)(B) [55]	LC	70.6 / 73.0
PMF [78]	LC	- / 58.2
SalsaNext [8]	L	55.8 / -
Realsurf [55]	L	67.6 / -
SPVCNN++ [56]	L	67.7 / -
VueNet3D [55]	L	68.6 / -
SphereFormer [31]	L	- / 69.9
Ours (Student w.o KD)	L	68.2 / 66.5
Ours (Student w KD)	L	**69.5 / 68.7**
Ours (Teacher)	L	71.3 / 69.8

Table 4: Quantitative Results of Different Approaches on Waymo Open Dataset. The modalities available on Waymo include LiDAR(L), and Camera(C).

translates to a 1.64× faster inference time (0.0362s vs. 0.0592s) and a 1.64× higher FPS (27.70 vs. 16.90), with a 1.68× reduction in batch inference time, making it suitable for real-time applications. Additionally, Student uses 4.5× less peak CUDA memory (3.57 GB vs 16.05 GB), which benefits more from Flash Attention optimizations. In terms of time and memory usage, the total CPU time of the teacher (501.109 ms) and the CUDA time (427.305 ms) are 2.47× and 4.19× higher than that of the student (203.096 ms, 102.068 ms), respectively. At the operational level, the teacher's MM_{add} operation consumes 16.05 GB of CUDA memory and 173.506 ms, which are 4.5× and 5.0× more than the student's 3.57 GB and 34.749 ms. The Teacher also requires 2.91× to 4.69× more memory for operations like Alloc, Idx, and LN, underscoring its higher resource demands. Although the Teacher excels in accuracy on high performance hardware, the Student's reduced memory footprint and faster execution make it ideal for real-time deployment on resource-constrained edge devices, competitive with efficient non-KD models like SparseConv [7] and KPConv [57], with potential accuracy trade-offs worth exploring further.

5 Discussion and Future Work

This work demonstrates that incorporating topological priors and gradient-guided feature alignment significantly enhances the knowledge distillation process for point-cloud semantic segmentation. Using structural insights from persistent homology and prioritizing tasks-relevant features, the proposed student model achieves a strong trade-off between accuracy and efficiency, making it highly suitable for deployment in resource-constrained settings.

Metric	**Teacher Model (46.16M params)**	**Student Model (2.78M params)**	**Comparison**
Total Parameters	46,160,000 (∼46.16M)	2,780,000 (∼2.78M)	Student is 16.6× smaller
Encoder Depths	(2, 2, 2, 6, 2) (14 blocks)	(1, 1, 1, 2, 1) (6 blocks)	Student has 2.33× fewer blocks
Encoder Channels	(32, 64, 128, 256, 512)	(16, 16, 32, 64, 128)	Student channels 2×-4× smaller
Encoder Attention Heads	(2, 4, 8, 16, 32)	(1, 1, 2, 4, 8)	Student heads 2×-4× fewer
Decoder Depths	(2, 2, 2, 2) (8 blocks)	(1, 1, 1, 1) (4 blocks)	Student has 2× fewer blocks
Decoder Channels	(64, 64, 128, 256)	(64, 64, 128, 128)	Student last stage 2× smaller
Decoder Attention Heads	(4, 4, 8, 16)	(2, 2, 4, 8)	Student heads 2× fewer
Patch Size	1024	1024	Same
Encoder (GFLOPs)	380.25	10.36	Student is 36.70× lower
Decoder (GFLOPs)	116.44	33.45	Student is 3.48× lower
Total Attention Compute (Encoder)	22.58	0.60	Student is 37.63× lower
Inference Time (Excl. Overhead)	∼0.0592s	∼0.0362s	Speedup: 1.64×
Batch Time Inference	∼7.34s	∼4.38s	Student consistently faster
FPS	∼16.90	∼27.70	Student 1.64× higher FPS
Fixed Overhead	∼0.018s	∼0.011s	Speed up: 1.58×
Attention Mechanism	Flash Attention enabled	Flash Attention enabled	Student benefits more from Flash Attention

Table 5: Comparison between Teacher and Student Models on NuScenes.

Metric	**Teacher Model (46.16M params)**	**Student Model (2.78M params)**	**Comparison**
Total CPU Time[b]	501.109 ms	203.096 ms	298.013 ms (2.47×)
Total CUDA Time	427.305 ms	102.068 ms	325.237 ms (4.19×)
MM$_{\text{add}}$ (CUDA Memory)[a]	16.05 GB	3.57 GB	12.48 GB (4.5×)
MM$_{\text{add}}$ (Self CUDA Time)[a]	173.506 ms	34.749 ms	138.757 ms (5.0×)
Alloc (CUDA Memory)	8.73 GB	3.00 GB	5.73 GB (2.91×)
Idx (CUDA Memory)	7.27 GB	1.78 GB	5.49 GB (4.08×)
GELU (CUDA Memory)	6.82 GB	1.67 GB	5.15 GB (4.08×)
LN (CUDA Memory)[a]	4.62 GB	985.43 MB	3.66 GB (4.69×)
Infer (Self CPU Time)	47.008 ms	37.243 ms	9.765 ms (1.26×)
MM$_{\text{add}}$ (Self CPU Time)[a]	5.402 ms	2.715 ms	2.687 ms (1.99×)

a - Operations contributing to attention layers (e.g., matrix multiplications for Q, K, V computations, and layer normalization).

b - Total CPU Time is reported from the profiling run with CUDA time measurements; a separate memory-focused run reports 278.804 ms (Teacher) and 92.436 ms (Student), yielding a 3.02× ratio.

Table 6: Memory and Time Usage Comparison between Teacher and Student Models.

However, there are several directions worth exploring further. First, while the topology-aware loss effectively captures global geometric structures, it may be sensitive to the filtration scale used in persistence diagram computation. Future work could investigate adaptive or learned filtration strategies to improve robustness across diverse scene types. Second, although the student model generalizes well across multiple datasets, its reliance on a fixed student architecture may limit flexibility. Exploring neural architecture search or adapting a task-aware model could offer additional performance gains. Finally, our method currently distills knowledge in a one-to-one teacher-student setup; extending this to multi-teacher or collaborative distillation frameworks or exploring a one-stage joint training paradigm, where the teacher and student are optimized simultaneously, could further streamline the training process and improve representation alignment could further enhance generalization, especially in complex outdoor environments.

Unlike traditional tools such as Ripser++ [71], which construct Vietoris-Rips complexes through a full filtration from $\epsilon = 0$ to a maximum threshold, our implementation approximates topological characteristics at multiple fixed scales to ensure efficiency and differentiability within neural pipelines. Although this snapshot-based approach may not capture all intermediate birth-and-death pairs, it provides sufficient coverage across representative scales while keeping the computational overhead manageable.

References

[1] Jens Behley, Martin Garbade, Andres Milioto, Jonas Quenzel, Sven Behnke, Cyrill Stachniss, and Jurgen Gall. Semantickitti: A dataset for semantic scene understanding of lidar sequences. *Proceedings of the IEEE International Conference on Computer Vision (ICCV)*, pages 9297–9307, 2019.

[2] Holger Caesar, Alex Bankiti, Alexander H Lang, Sourabh Vora, Venice Erin Liong, Qiang Xu, Anush Krishnan, Yu Pan, Giancarlo Baldan, and Oscar Beijbom. nuscenes: A multimodal dataset for autonomous driving. *Proceedings of the IEEE Conference on Computer Vision and Pattern Recognition (CVPR)*, pages 11621–11631, 2020.

[3] Chao Cao, Marius Preda, and Titus Zaharia. 3d point cloud compression: A survey. In *Proceedings of the 24th International Conference on 3D Web Technology*, Web3D '19, page 1–9, New York, NY, USA, 2019. Association for Computing Machinery.

[4] Jun Cen, Shiwei Zhang, Yixuan Pei, Kun Li, Hang Zheng, Maochun Luo, Yingya Zhang, and Qifeng Chen. Cmdfusion: Bidirectional fusion network with cross-modality knowledge distillation for lidar semantic segmentation. *IEEE Robotics and Automation Letters*, 9(1):771–778, 2024.

[5] Xiaozhi Chen, Huimin Ma, Ji Wan, Bo Li, and Tian Xia. Multi-view 3d object detection network for autonomous driving. In *Proceedings of the IEEE conference on Computer Vision and Pattern Recognition*, pages 1907–1915, 2017.

[6] Jungwook Choi, Swagath Venkataramani, Vijayalakshmi (Viji) Srinivasan, Kailash Gopalakrishnan, Zhuo Wang, and Pierce Chuang. Accurate and efficient 2-bit quantized neural networks. In A. Talwalkar, V. Smith, and M. Zaharia, editors, *Proceedings of Machine Learning and Systems*, volume 1, pages 348–359, 2019.

[7] Christopher Choy, JunYoung Gwak, and Silvio Savarese. 4d spatio-temporal convnets: Minkowski convolutional neural networks. In *Proceedings of the IEEE/CVF conference on computer vision and pattern recognition*, pages 3075–3084, 2019.

[8] Tiago Cortinhal, George Tzelepis, and Eren Erdal Aksoy. SalsaNext: Fast, Uncertainty-Aware Semantic Segmentation of LiDAR Point Clouds. In *Advances in Visual Computing: 15th International Symposium, ISVC 2020, San Diego, CA, USA, October 5–7, 2020, Proceedings, Part II*, volume 12510 of *Lecture Notes in Computer Science*, pages 207–222. Springer, 2020.

[9] Tiago Cortinhal, George Tzelepis, and Eren Erdal Aksoy. Salsanext: Fast, uncertainty-aware semantic segmentation of lidar point clouds. In *Advances in Visual Computing: 15th International Symposium, ISVC 2020, San Diego, CA, USA, October 5–7, 2020, Proceedings, Part II 15*, pages 207–222. Springer, 2020.

[10] Runpei Dong, Zhanhong Tan, Mengdi Wu, Linfeng Zhang, and Kaisheng Ma. Finding the task-optimal low-bit sub-distribution in deep neural networks. In *International Conference on Machine Learning*, pages 5343–5359. PMLR, 2022.

[11] Andreas Geiger, Philip Lenz, and Raquel Urtasun. Are we ready for autonomous driving? the kitti vision benchmark suite. In *2012 IEEE conference on computer vision and pattern recognition*, pages 3354–3361. IEEE, 2012.

[12] Martin Gerdzhev, Ryan Razani, Ehsan Taghavi, and Liu Bingbing. Tornado-net: multiview total variation semantic segmentation with diamond inception module. In *2021 IEEE International Conference on Robotics and Automation (ICRA)*, pages 9543–9549. IEEE, 2021.

[13] Tim Golla and Reinhard Klein. Real-time point cloud compression. In *2015 IEEE/RSJ International Conference on Intelligent Robots and Systems (IROS)*, pages 5087–5092, 2015.

[14] Ruben Gomez-Ojeda, Jesus Briales, and Javier Gonzalez-Jimenez. Pl-svo: Semi-direct monocular visual odometry by combining points and line segments. In *2016 IEEE/RSJ International Conference on Intelligent Robots and Systems (IROS)*, pages 4211–4216. IEEE, 2016.

[15] Meng-Hao Guo, Jun-Xiong Cai, Zheng-Ning Liu, Tai-Jiang Mu, Ralph R Martin, and Shi-Min Hu. Pct: Point cloud transformer. *Computational Visual Media*, 7:187–199, 2021.

[16] Xiaoyang Guo, Shaoshuai Shi, Xiaogang Wang, and Hongsheng Li. Liga-stereo: Learning lidar geometry aware representations for stereo-based 3d detector. In *Proceedings of the IEEE/CVF international conference on computer vision*, pages 3153–3163, 2021.

[17] Sangchul Hahn and Heeyoul Choi. Self-knowledge distillation in natural language processing. In *Proceedings of the International Conference on Recent Advances in Natural Language Processing (RANLP)*, pages 423–430, 2019.

[18] Dan Halperin and Niklas Eisl. Point cloud based scene segmentation: A survey, 2025.

[19] Song Han, Huizi Mao, and William J. Dally. Deep compression: Compressing deep neural networks with pruning, trained quantization and huffman coding. In *Proceedings of the International Conference on Learning Representations (ICLR)*, 2016.

[20] Haoyu He, Xingjian Shi, Jonas Mueller, Sheng Zha, Mu Li, and George Karypis. Distiller: A systematic study of model distillation methods in natural language processing. In *Proceedings of the Second Workshop on Simple and Efficient Natural Language Processing*, pages 119–133, Virtual, 2021. Association for Computational Linguistics.

[21] Geoffrey Hinton, Oriol Vinyals, and Jeff Dean. Distilling the knowledge in a neural network. In *Advances in Neural Information Processing Systems (NeurIPS)*, pages 1–2, 2014.

[22] Geoffrey Hinton, Oriol Vinyals, and Jeff Dean. Distilling the knowledge in a neural network. *arXiv preprint arXiv:1503.02531*, 2015.

[23] Yuenan Hou, Xinge Zhu, Yuexin Ma, Chen Change Loy, and Yikang Li. Point-to-voxel knowledge distillation for lidar semantic segmentation. In *Proceedings of the IEEE/CVF conference on computer vision and pattern recognition*, pages 8479–8488, 2022.

[24] Yuenan Hou, Xinge Zhu, Yuexin Ma, Chen Change Loy, and Yikang Li. Point-to-voxel knowledge distillation for lidar semantic segmentation. In *Proceedings of the IEEE/CVF Conference on Computer Vision and Pattern Recognition (CVPR)*, pages 8479–8488, June 2022.

[25] Yuenan Hou, Xinge Zhu, Yuexin Ma, Chen Change Loy, and Yikang Li. Point-to-voxel knowledge distillation for lidar semantic segmentation. In *Proceedings of the IEEE/CVF conference on computer vision and pattern recognition*, pages 8479–8488, 2022.

[26] Andrew Howard, Mark Sandler, Grace Chu, Liang-Chieh Chen, Bo Chen, Mingxing Tan, Weijun Wang, Yukun Zhu, Ruoming Pang, Vijay Vasudevan, et al. Searching for mobilenetv3. In *Proceedings of the IEEE/CVF international conference on computer vision*, pages 1314–1324, 2019.

[27] Eun Som Jeon, Rahul Khurana, Aishani Pathak, and Pavan Turaga. Leveraging topological guidance for improved knowledge distillation. In *Proceedings of the ICML 2024 Workshop on Geometry-grounded Representation Learning and Generative Modeling*, 2024.

[28] Jungeun Kim, Junwon You, Dongjin Lee, Ha Young Kim, and Jae-Hun Jung. Do topological characteristics help in knowledge distillation? In *Forty-first International Conference on Machine Learning*, 2024.

[29] Deyvid Kochanov, Fatemeh Karimi Nejadasl, and Olaf Booij. Kprnet: Improving projection-based lidar semantic segmentation. *arXiv preprint arXiv:2007.12668*, 2020.

[30] Solomon Kullback. Kullback-leibler divergence, 1951.

[31] Xin Lai, Yukang Chen, Fanbin Lu, Jianhui Liu, and Jiaya Jia. Spherical transformer for lidar-based 3d recognition. In *Proceedings of the IEEE/CVF Conference on Computer Vision and Pattern Recognition (CVPR)*, pages 17545–17555, 2023.

[32] Qizhen Lan and Qing Tian. Gradient-guided knowledge distillation for object detectors. In *Proceedings of the IEEE/CVF Winter Conference on Applications of Computer Vision (WACV)*, pages 423–432, 2024.

[33] Alex H Lang, Sourabh Vora, Holger Caesar, Lubing Zhou, Jiong Yang, and Oscar Beijbom. Pointpillars: Fast encoders for object detection from point clouds. In *Proceedings of the IEEE/CVF conference on computer vision and pattern recognition*, pages 12697–12705, 2019.

[34] Bo Li, Tianlei Zhang, and Tian Xia. Vehicle detection from 3d lidar using fully convolutional network. In *Proceedings of Robotics: Science and Systems (RSS)*, 2016.

[35] Jia-Chen Li, Jun-Guo Lu, Ming Wei, Hong-Yi Kang, and Qing-Hao Zhang. Tpv-igkd: Image-guided knowledge distillation for 3d semantic segmentation with tri-plane-view. *IEEE Transactions on Intelligent Transportation Systems*, 25(8):10405–10416, 2024.

[36] Jiale Li, Hang Dai, and Yong Ding. Self-distillation for robust lidar semantic segmentation in autonomous driving. In *European conference on computer vision*, pages 659–676. Springer, 2022.

[37] Jiale Li, Hang Dai, Hao Han, and Yong Ding. Mseg3d: Multimodal 3d semantic segmentation for autonomous driving. In *Proceedings of the IEEE/CVF Conference on Computer Vision and Pattern Recognition (CVPR)*, pages 21694–21704, 2023.

[38] Venice Erin Liong, Thi Ngoc Tho Nguyen, Sergi Widjaja, Dhananjai Sharma, and Zhuang Jie Chong. Amvnet: Assertion-based multi-view fusion network for lidar semantic segmentation. *CoRR*, abs/2012.04934, 2020.

[39] Yifan Liu, Ke Chen, Chris Liu, Zengchang Qin, Zhenbo Luo, and Jingdong Wang. Structured knowledge distillation for semantic segmentation. In *Proceedings of the IEEE/CVF conference on computer vision and pattern recognition*, pages 2604–2613, 2019.

[40] Zechun Liu, Haoyuan Mu, Xiangyu Zhang, Zichao Guo, Xin Yang, Kwang-Ting Cheng, and Jian Sun. Metapruning: Meta learning for automatic neural network channel pruning. In *Proceedings of the IEEE/CVF international conference on computer vision*, pages 3296–3305, 2019.

[41] Christos Louizos, Max Welling, and Diederik P. Kingma. Learning sparse neural networks through l_0 regularization. In *Proceedings of the International Conference on Learning Representations (ICLR)*, 2018.

[42] Ningning Ma, Xiangyu Zhang, Hai-Tao Zheng, and Jian Sun. Shufflenet v2: Practical guidelines for efficient cnn architecture design. In *Proceedings of the European conference on computer vision (ECCV)*, pages 116–131, 2018.

[43] Xu Ma, Can Qin, Haoxuan You, Haoxi Ran, and Yun Fu. Rethinking network design and local geometry in point cloud: A simple residual mlp framework. In *Proceedings of the International Conference on Learning Representations (ICLR)*, 2022.

[44] Andres Milioto, Ignacio Vizzo, Jens Behley, and Cyrill Stachniss. Rangenet++: Fast and accurate lidar semantic segmentation. In *2019 IEEE/RSJ international conference on intelligent robots and systems (IROS)*, pages 4213–4220. IEEE, 2019.

[45] Markus Nagel, Mart van Baalen, Tijmen Blankevoort, and Max Welling. Data-free quantization through weight equalization and bias correction. In *Proceedings of the IEEE/CVF International Conference on Computer Vision*, pages 1325–1334, 2019.

[46] Yong-Joo Oh and Yoshio Watanabe. Development of small robot for home floor cleaning. In *Proceedings of the 41st SICE Annual Conference. SICE 2002.*, volume 5, pages 3222–3223. IEEE, 2002.

[47] Charles R Qi, Hao Su, Kaichun Mo, and Leonidas J Guibas. Pointnet: Deep learning on point sets for 3d classification and segmentation. In *Proceedings of the IEEE conference on computer vision and pattern recognition*, pages 652–660, 2017.

[48] Haibo Qiu, Baosheng Yu, and Dacheng Tao. Gfnet: Geometric flow network for 3d point cloud semantic segmentation. *arXiv preprint arXiv:2207.02605*, 2022.

[49] Ahmad Rashid, Vasileios Lioutas, Abbas Ghaddar, and Mehdi Rezagholizadeh. Towards zero-shot knowledge distillation for natural language processing. In *Proceedings of the 2021 Conference on Empirical Methods in Natural Language Processing (EMNLP)*, pages 6551–6561, 2021.

[50] Damien Robert, Hugo Raguet, and Loic Landrieu. Efficient 3d semantic segmentation with superpoint transformer. In *Proceedings of the IEEE/CVF International Conference on Computer Vision*, pages 17195–17204, 2023.

[51] Adriana Romero, Nicolas Ballas, Samira Ebrahimi Kahou, Antoine Chassang, Carlo Gatta, and Yoshua Bengio. Fitnets: Hints for thin deep nets. In Yoshua Bengio and Yann LeCun, editors, *3rd International Conference on Learning Representations, ICLR 2015, San Diego, CA, USA, May 7-9, 2015, Conference Track Proceedings*, 2015.

[52] Victor Sanh, Lysandre Debut, Julien Chaumond, and Thomas Wolf. Distilbert, a distilled version of BERT: Smaller, faster, cheaper and lighter. *arXiv preprint arXiv:1910.01108*, pages 1–2, 2019.

[53] Shuran Song, Fisher Yu, Andy Zeng, Angel X Chang, Manolis Savva, and Thomas Funkhouser. Semantic scene completion from a single depth image. In *Proceedings of the IEEE conference on computer vision and pattern recognition*, pages 1746–1754, 2017.

[54] Pei Sun, Henrik Kretzschmar, Xerxes Dotiwalla, Alexandre Chouard, Anand Patnaik, Paul Tsui, Yin Guo, Yuning Zhou, Yuning Chai, Benjamin Caine, et al. Scalability in perception for autonomous driving: Waymo open dataset. *Proceedings of the IEEE Conference on Computer Vision and Pattern Recognition (CVPR)*, pages 2446–2454, 2020.

[55] Tianfang Sun, Zhizhong Zhang, Xin Tan, Yong Peng, Yanyun Qu, and Yuan Xie. Uni-to-multi modal knowledge distillation for bidirectional lidar-camera semantic segmentation. *IEEE Transactions on Pattern Analysis and Machine Intelligence*, 46(12):11059–11072, 2024.

[56] Haotian Tang, Zhijian Liu, Shengyu Zhao, Yujun Lin, Ji Lin, Hanrui Wang, and Song Han. Searching efficient 3d architectures with sparse point-voxel convolution. In *Computer Vision – ECCV 2020: 16th European Conference, Glasgow, UK, August 23–28, 2020, Proceedings, Part XXVIII*, volume 12373 of *Lecture Notes in Computer Science*, pages 685–702. Springer, 2020.

[57] Hugues Thomas, Charles R Qi, Jean-Emmanuel Deschaud, Beatriz Marcotegui, François Goulette, and Leonidas J Guibas. Kpconv: Flexible and deformable convolution for point clouds. In *Proceedings of the IEEE/CVF international conference on computer vision*, pages 6411–6420, 2019.

[58] Frederick Tung and Greg Mori. Similarity-preserving knowledge distillation. In *Proceedings of the IEEE/CVF international conference on computer vision*, pages 1365–1374, 2019.

[59] Cédric Villani. *Optimal Transport: Old and New*, volume 338 of *Grundlehren der mathematischen Wissenschaften*. Springer, 2009.

[60] Peng-Shuai Wang, Yang Liu, Yu-Xiao Guo, Chun-Yu Sun, and Xin Tong. O-cnn: Octree-based convolutional neural networks for 3d shape analysis. *ACM Transactions On Graphics (TOG)*, 36(4):1–11, 2017.

[61] Xiaoyang Wu, Li Jiang, Peng-Shuai Wang, Zhijian Liu, Xihui Liu, Yu Qiao, Wanli Ouyang, Tong He, and Hengshuang Zhao. Point transformer v3: Simpler, faster, stronger. In *2024 IEEE/CVF Conference on Computer Vision and Pattern Recognition (CVPR)*, pages 4840–4851, 2024.

[62] Xiaoyang Wu, Yixing Lao, Li Jiang, Xihui Liu, and Hengshuang Zhao. Point transformer v2: Grouped vector attention and partition-based pooling. *Advances in Neural Information Processing Systems*, 35:33330–33342, 2022.

[63] Xiaoyang Wu, Yixing Lao, Li Jiang, Xihui Liu, and Hengshuang Zhao. Point transformer v2: Grouped vector attention and partition-based pooling. In *Advances in Neural Information Processing Systems (NeurIPS)*, 2022.

[64] Jianyun Xu, Ruixiang Zhang, Jian Dou, Yushi Zhu, Jie Sun, and Shiliang Pu. Rpvnet: A deep and efficient range-point-voxel fusion network for lidar point cloud segmentation. In *Proceedings of the IEEE/CVF international conference on computer vision*, pages 16024–16033, 2021.

[65] Xu Yan, Jiantao Gao, Chaoda Zheng, Chao Zheng, Ruimao Zhang, Shuguang Cui, and Zhen Li. 2dpass: 2d priors assisted semantic segmentation on lidar point clouds. In *European Conference on Computer Vision*, pages 677–695. Springer, 2022.

[66] Yu-Qi Yang, Yu-Xiao Guo, Jian-Yu Xiong, Yang Liu, Hao Pan, Peng-Shuai Wang, Xin Tong, and Baining Guo. Swin3d: A pretrained transformer backbone for 3d indoor scene understanding. *arXiv preprint arXiv:2304.06906*, 2023.

[67] Dongqiangzi Ye, Zixiang Zhou, Weijia Chen, Yufei Xie, Yu Wang, Panqu Wang, and Hassan Foroosh. Lidarmultinet: Towards a unified multi-task network for lidar perception. *arXiv preprint arXiv:2209.09385*, 2022.

[68] Feihu Zhang, Jin Fang, Benjamin Wah, and Philip Torr. Deep fusionnet for point cloud semantic segmentation. In *Computer Vision–ECCV 2020: 16th European Conference, Glasgow, UK, August 23–28, 2020, Proceedings, Part XXIV 16*, pages 644–663. Springer, 2020.

[69] Linfeng Zhang, Runpei Dong, Hung-Shuo Tai, and Kaisheng Ma. Pointdistiller: Structured knowledge distillation towards efficient and compact 3d detection. In *Proceedings of the IEEE/CVF Conference on Computer Vision and Pattern Recognition (CVPR)*, pages 21791–21801, June 2023.

[70] S. Zhang, J. Deng, L. Bai, et al. Hvdistill: Transferring knowledge from images to point clouds via unsupervised hybrid-view distillation. *International Journal of Computer Vision*, 132:2585–2599, 2024.

[71] Simon Zhang, Mengbai Xiao, and Hao Wang. Gpu-accelerated computation of vietoris-rips persistence barcodes. In *36th International Symposium on Computational Geometry (SoCG 2020)*. Schloss Dagstuhl-Leibniz-Zentrum für Informatik, 2020.

[72] Yang Zhang, Zixiang Zhou, Philip David, Xiangyu Yue, Zerong Xi, Boqing Gong, and Hassan Foroosh. Polarnet: An improved grid representation for online lidar point clouds semantic segmentation. In *Proceedings of the IEEE/CVF conference on computer vision and pattern recognition*, pages 9601–9610, 2020.

[73] Hengshuang Zhao, Li Jiang, Chi-Wing Fu, and Jiaya Jia. Pointweb: Enhancing local neighborhood features for point cloud processing. In *Proceedings of the IEEE/CVF conference on computer vision and pattern recognition*, pages 5565–5573, 2019.

[74] Hengshuang Zhao, Li Jiang, Jiaya Jia, Philip H. S. Torr, and Vladlen Koltun. Point transformer. In *Proceedings of the IEEE/CVF International Conference on Computer Vision (ICCV)*, pages 16259–16268, 2021.

[75] Lin Zhao, Siyuan Xu, Liman Liu, Delie Ming, and Wenbing Tao. Svaseg: Sparse voxel-based attention for 3d lidar point cloud semantic segmentation. *Remote Sensing*, 14(18):4471, 2022.

[76] Yin Zhou and Oncel Tuzel. Voxelnet: End-to-end learning for point cloud based 3d object detection. In *Proceedings of the IEEE Conference on Computer Vision and Pattern Recognition (CVPR)*, June 2018.

[77] Xinge Zhu, Hui Zhou, Tai Wang, Fangzhou Hong, Yuexin Ma, Wei Li, Hongsheng Li, and Dahua Lin. Cylindrical and asymmetrical 3d convolution networks for lidar segmentation. In *Proceedings of the IEEE/CVF conference on computer vision and pattern recognition*, pages 9939–9948, 2021.

[78] Zhuangwei Zhuang, Rong Li, Kui Jia, Qicheng Wang, Yuanqing Li, and Mingkui Tan. Perception-aware multi-sensor fusion for 3d lidar semantic segmentation. In *Proceedings of the IEEE/CVF International Conference on Computer Vision (ICCV)*, pages 16280–16290, 2021.

A Experimental Details

A.1 Dataset Details

SemanticKITTI [1] provides LiDAR point clouds from urban and suburban scenes, featuring 22 sequences with dense semantic annotations across 19 classes (e.g., vehicles, pedestrians, roads). Its high resolution and detailed labels make it a rigorous testbed for semantic segmentation.

NuScenes [2] integrates LiDAR, camera, and radar data in 1,000 diverse scenes, including urban roads and highways. With 3D bounding box annotations for 23 object types, it challenges models with varied weather, occlusions, and dynamic elements suited for detection and segmentation tasks. In addition, we use nuScenes-lidar seg, which is an extension of nuScenes. This dataset has semantic labels of 32 categories and annotates each point from keyframes in nuScenes. We used the 700 scenes in the training set with segmentation labels to fine-tune for the semantic segmentation task, and the 150 scenes in the validation set to verify the performance.

Waymo Open Dataset [54] delivers high-resolution LiDAR data from 1,000 segments in various locations, with frequent sweeps and 3D annotations for vehicles, pedestrians and cyclists. Its long-range scans and varied conditions test robustness and generalization.

Training Details. We apply the same setting to all datasets mentioned with a batch size of 12 for training, 18 for validation, and 1 for testing. The training process is trained with 50 epochs, with evaluations performed at every epoch. We use the AdamW optimizer with an initial learning rate of 0.002 and a weight decay of 0.005. The training process follows a OneCycleLR learning rate scheduling strategy, which dynamically adjusts the learning rate throughout the training cycle. Initially, the learning rate increases rapidly to a pre-defined maximum value during the warm-up phase, ensuring a stable convergence. Then it follows a cosine annealing schedule, gradually decreasing to a much lower value as the training progresses. This approach helps the model escape sharp local minima early in training, while allowing fine-tuning in later stages for better generalization. In addition, a cyclical adjustment to weight decay prevents overfitting and improves the robustness of the model. Data augmentation techniques are applied during training, such as random rotation, scaling, flipping, and jittering. The evaluation pipeline includes a semantic segmentation evaluator and a precise evaluator, ensuring a reliable model evaluation.

A.2 Model and Training Hyperparameters

In our experiments, we use Point Transformer V3 [61] as both the teacher and the student backbone, the student model being significantly reduced in capacity to enhance efficiency while maintaining essential representational power. Note that at the time of this project, the authors have not yet released the final weights for the model Point Transformer V3, so we have trained them from scratch. The student network is approximately 20% the depth of the teacher. Specifically, the encoder of the student model has shallower depths, which reduce from teacher $(2, 2, 2, 6, 2)$ to $(1, 1, 1, 2, 1)$. Similarly, the channel dimensions are reduced from $(32, 64, 128, 256, 512)$ in the teacher to $(16, 16, 32, 64, 128)$ in the student. The number of attention heads in the transformer layers is systematically reduced from the teacher's (2, 4, 8, 16, 32) to (1, 1, 2, 4, 8) across the five encoder stages, effectively halving the complexity of multi-head attention at each stage. This reduction reduces the computational load while preserving the transformer's capacity to model spatial relationships. The decoder follows a similar strategy, with depths of (1, 1, 1, 1), channels of (64, 64, 128, 128) and attention heads scaled down from the teacher's (4, 4, 8, 16) to (2, 2, 4, 8) in its four stages, ensuring a proportional decrease.

By retaining strides of (2, 2, 2, 2) and a patch size of 1024, the student model maintains structural compatibility for effective distillation.

Training is carried out on multiple datasets, including nuScenes, SemanticKITTI, and Waymo, using cross-entropy and Lovász segmentation losses to optimize segmentation performance. We adopt a two-stage distillation strategy in which the teacher model is first trained to full performance before being used to guide the student model in a separate distillation phase. This approach ensures that the student benefits from a fully converged and stable teacher during knowledge transfer.

For topology-aware learning, we use Vietoris-Rips filtration to compute persistence diagrams, enabling robust topological feature extraction across point-cloud datasets. This choice ensures that meaningful topological structures are captured, while preventing excessive noise in the persistence diagrams. The filtration scale was empirically determined to balance computational efficiency and representational fidelity. Using this set-up, we ensure that the student model effectively learns both the geometric and topological structures necessary for accurate point-cloud segmentation.

A.3 Data Augmentation

To enhance the robustness and generalization ability of the model, we applied a series of data augmentation techniques during training. Specifically, the input point clouds were randomly rotated around the z-axis within a range of $\pm 1^\circ$ with a probability of 0.5, and uniformly scaled by a random factor between 0.9 and 1.1. Random flipping was performed along spatial axes with a probability of 0.5 to introduce geometric variability. Additionally, Gaussian jittering with a standard deviation of 0.005 and a clipping value of 0.02 was applied to perturb point positions slightly. Following these augmentations, a grid sampling operation with a grid size of 0.05 m was used to downsample the point cloud, where hashing was performed using the Fowler–Noll–Vo (FNV) hash function. Finally, the processed data were converted into tensors and relevant features (coordinates and strength) along with labels (segment) were collected for training. These augmentations were designed to simulate realistic sensor noise and spatial variations, thereby improving the model's performance on unseen data.

B Details of Resources Used

We conducted all experiments on the University HPC Cluster using NVIDIA A100. Each node is equipped with 2 NVIDIA A100 GPUs (81 GB VRAM each), and we utilized one node and one A100 GPU for training and evaluation. The cluster runs on a Linux environment with Slurm for job scheduling.

C Theoretical Justification of Topology-Aware Distillation

C.1 Convergence of Chamfer Distance to 2-Wasserstein Distance

In our framework, we adopt the Chamfer distance ($\mathcal{L}_{\text{CD}}$) to measure the similarity between persistence diagrams due to its efficiency and differentiability. Here, we theoretically justify this choice.

Theorem 1. *Let D_T and D_S be the persistence diagrams for the teacher and student models, respectively. If $\mathcal{L}_{CD}(D_T, D_S) \to 0$, then the 2-Wasserstein distance between D_T and D_S also converges:*

$$W_2(D_T, D_S) \leq \sqrt{\mathcal{L}_{CD}(D_T, D_S)}. \tag{7}$$

Thus, minimizing Chamfer Distance implicitly minimizes the Wasserstein distance between persistence diagrams, ensuring topological consistency.

Proof. By the properties of optimal transport [59], the 2-Wasserstein distance between persistence diagrams satisfies:

$$W_2^2(D_T, D_S) = \inf_{\gamma \in \Gamma(D_T, D_S)} \sum_{(p,q) \in \gamma} \|p - q\|^2, \tag{8}$$

where $\Gamma(D_T, D_S)$ denotes the set of all valid matchings. The Chamfer Distance relaxes this formulation by independently matching each point to its nearest neighbor:

$$\mathcal{L}_{\text{CD}}(D_T, D_S) = \sum_{p \in D_T} \min_{q \in D_S} \|p - q\|^2 + \sum_{q \in D_S} \min_{p \in D_T} \|q - p\|^2. \tag{9}$$

Since $\mathcal{L}_{\text{CD}}$ considers all bidirectional nearest neighbors, it provides an upper bound on $W_2^2(D_T, D_S)$. Taking the square root completes the proof. □

C.2 Practical Motivation for Using Chamfer Distance

Although the 2-Wasserstein distance (W_2) is the standard metric to compare persistence diagrams in topological data analysis, we opt for the Chamfer Distance ($\mathcal{L}_{\text{CD}}$) due to the following reasons:

- **Computational Efficiency**: Computing W_2 requires solving an optimal transport problem with complexity $O(n^3 \log n)$, which is prohibitively expensive for large persistence diagrams derived from dense 3D point clouds. In contrast, the Chamfer distance can be computed in $O(nm)$ time via nearest-neighbor search.
- **Differentiability**: The Chamfer distance is readily differentiable, enabling direct integration with gradient-based optimization. Wasserstein distance typically requires approximations (e.g., Sinkhorn regularization), introducing additional hyperparameters and potential training instability.
- **Empirical Stability**: In our experiments, Chamfer Distance yields stable convergence during training and maintains consistent topological structures without the need for complex approximations.

C.3 Controlling Topology Loss Influence

To prevent the topology loss $\mathcal{L}_{\text{topo}}$ from dominating the overall training dynamics, we impose a gradient norm constraint:

$$\|\nabla_x \mathcal{L}_{\text{topo}}\| \leq \alpha \|\nabla_x \mathcal{L}_{\text{feat}}\|, \tag{10}$$

where $\alpha > 0$ is a small hyperparameter. This ensures that topology-aware regularization complements rather than overwhelms feature-based alignment.

C.4 Visualization of Topology-Aware Analysis

Figure 3 illustrates how persistent homology captures the evolution of topological features across different filtration scales. Given a point cloud, we construct a simplicial complex and track the birth and death of topological structures as the filtration parameter ϵ increases. The persistence diagram $D = \{(b_i, d_i)\}_{i=1}^{M}$ quantifies these events, where each point represents a topological feature. Longer bars correspond to persistent structures that encode essential geometric patterns, while shorter bars typically represent noise or minor perturbations.

Visualizing the persistence diagrams allows us to better understand the types of geometric features captured by the teacher model, such as connected components (H_0), loops (H_1) and voids (H_2). By encouraging the student to mimic these persistent topological features through topology-aware distillation, we aim to transfer not only semantic knowledge but also the critical underlying geometric structures necessary for robust point-cloud understanding. This visualization supports the intuition behind our method, showing that topological summaries can effectively reflect meaningful geometric information beyond what is captured by the Euclidean feature alignment.

D Broader Impacts

Our work enables efficient point cloud processing on resource-constrained edge devices, achieving a 1.64× faster inference (Table 3) and 4.5× lower memory usage (Table 6). This facilitates real-time deployment in self-driving cars, potentially enhancing road safety through better obstacle detection and reducing costs to make autonomous vehicles more accessible. However, the student model's reduced accuracy (78.17% mIoU vs. 80.03% compared to the teacher's mIoU) may lead to errors in object detection, risking accidents if not carefully validated. Widespread adoption of autonomous vehicles might displace jobs in transportation, impacting drivers.

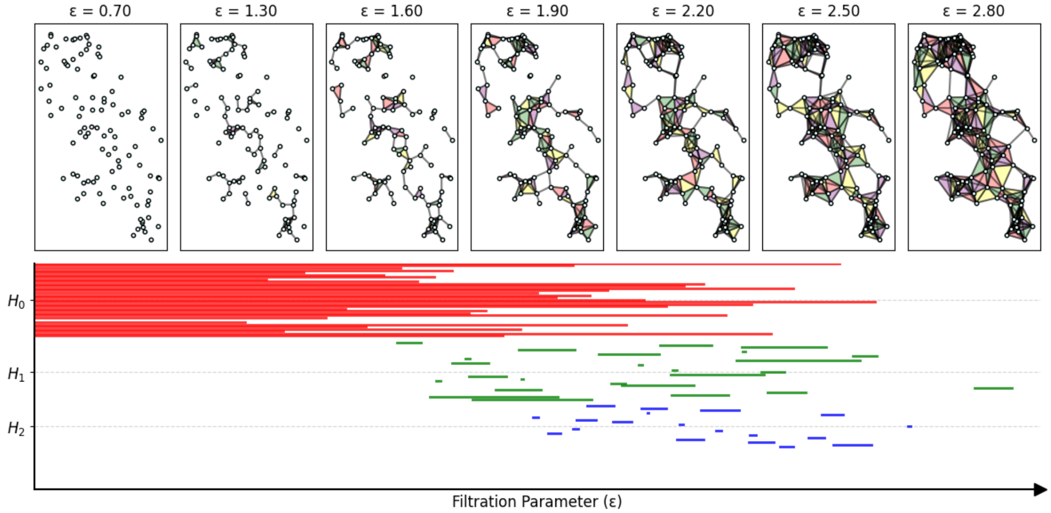

Figure 3: Illustration of topology-aware analysis through Vietoris–Rips filtration. The top row depicts the evolution of the simplicial complex as the filtration parameter ϵ increases. The bottom part shows the corresponding barcode representation of persistent homology groups in different dimensions (H_0, H_1, H_2).

E Ablation Study

Fig 4 shows a top-down view of the semantic segmentation results in the NuScene validation dataset. The student model demonstrates strong alignment with the ground truth across nearly all object classes, effectively capturing the spatial layout and fine-grained structures in the scene. Compared to the teacher, the student produces cleaner boundaries and more consistent predictions, particularly in regions with small or scattered objects. This highlights the effectiveness of our knowledge distillation approach in transferring knowledge while enhancing prediction quality.

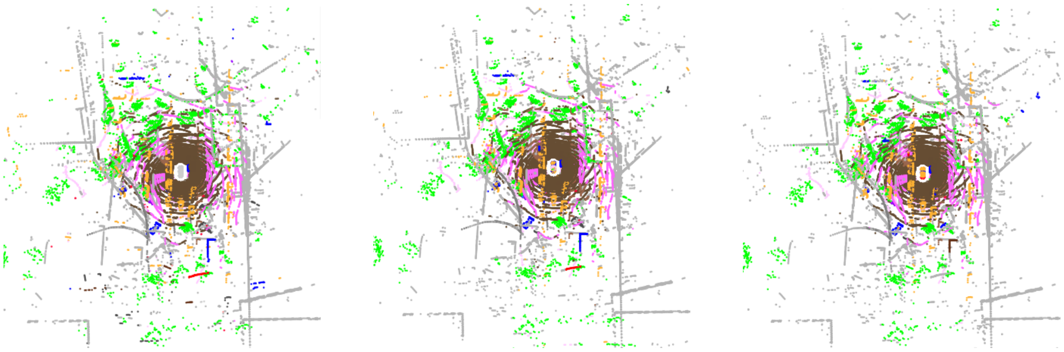

(a) Ground Truth

(b) Teacher Prediction

(c) Student Prediction

Figure 4: Visualization of our method on the nuScenes validation set. (a) Ground truth, (b) teacher model prediction, and (c) student model prediction. The student model closely follows the teacher's output and ground truth, successfully capturing almost all object classes, demonstrating the effectiveness of the knowledge distillation process.

The Table 7 clearly demonstrates the effectiveness of each proposed loss component in improving student model performance. Adding the loss with topology awareness $\mathcal{L}_{\text{topo}}$ to the baseline leads to significant improvements, particularly on Waymo (+3.5 mIoU) and SemanticKITTI (+1.7 mIoU), where the capture of the global geometric context is essential. Meanwhile, gradient-guided feature alignment loss $\mathcal{L}_{\text{grad}}$ yields consistent gains across datasets, with the most noticeable impact on nuScenes (+0.9 mIoU), highlighting its strength to refine local features and object boundaries. When combined in the full loss formulation, the student achieves the highest mIoU on all benchmarks, confirming the complementary nature of the preservation of global topology and the alignment of local characteristics. These results validate the ability of the proposed framework to distill both structural and task-relevant knowledge, allowing the lightweight student model to approach or even surpass the state-of-the-art performance while maintaining high efficiency.

$\mathcal{L}_{\text{KLD}}$	$\mathcal{L}_{\text{seg}}$	$\mathcal{L}_{\text{topo}}$	$\mathcal{L}_{\text{grad}}$	SemanticKITTI	Waymo	nuScenes
✓	✓			71.5	64.8	74.0
✓	✓	✓		73.2	68.3	77.3
✓	✓		✓	72.3	66.5	74.9
✓	✓	✓	✓	74.6	69.5	78.1

Table 7: Influence of each component on the final performance.